J Therm Spray Tech (2019) 28:53–62
https://doi.org/10.1007/s11666-018-0818-8

PEER REVIEWED

Plasma Spraying of Dense Ceramic Coating with Fully Bonded Lamellae Through Materials Design Based on the Critical Bonding Temperature Concept

Chang-Jiu Li[1] · Qi-Lan Zhang[1] · Shu-Wei Yao[1] · Guan-Jun Yang[1] · Cheng-Xin Li[1]

Submitted: 25 June 2018 / in revised form: 5 December 2018 / Published online: 2 January 2019

Abstract It is usually difficult to deposit a dense ceramic coating with fully bonded splats by plasma spraying at a room temperature. Following the recent research progress on the splat interface bonding formation, it was found that there is a well-defined relationship between the critical bonding temperature and the melting point of spray material. Thus, it can be proposed to control the lamellar bonding through the deposition temperature. In this study, to examine the feasibility of the bonding formation theory, a novel approach to the development of ceramic coating with dense microstructure by plasma spraying through materials design with a low melting point is proposed. Potassium titanate $K_2Ti_6O_{13}$ was selected as a typical ceramic material of a relatively low melting point for plasma spraying deposition of dense coating with well-bonded splats. Experiment was conducted by using $K_2Ti_6O_{13}$ for both splat and coating deposition. Results show that the splat is fully bonded with a ceramic substrate at room temperature, and the $K_2Ti_6O_{13}$ coating presents a dense microstructure and a fracture surface morphology similar to sintered bulk ceramic, revealing excellent inter-lamellar bonding formation. Moreover, both the hardness test and erosion test at 90° further confirmed the formation of the isotropic ceramic coating with fully bonded lamellae.

Keywords dense ceramic coatings · erosion behavior · $K_2Ti_6O_{13}$ · lamellae bonding · plasma spraying

This article is an invited paper selected from presentations at the 2018 International Thermal Spray Conference, held May 7-10, 2018, in Orlando, Florida, USA, and has been expanded from the original presentation.

✉ Chang-Jiu Li
licj@mail.xjtu.edu.cn

[1] State Key Laboratory for Mechanical Behavior of Materials, School of Materials Science and Engineering, Xi'an Jiaotong University, Xi'an 710049, Shaanxi, People's Republic of China

Introduction

Ceramic coatings have been widely used in different industrial fields (Ref 1). Different coating processes are employed to deposit ceramic coatings such as thermal spraying, physical vapor deposition, chemical vapor deposition, slurry coating, dip coating, and anodizing. Among all these processes, thermal spraying takes a two-third market share in the field of advanced ceramic coating fabrication in North America based on a survey report (Ref 2). It is evident that thermal spraying is one of the most important processes to deposit advanced ceramic coatings.

Plasma spraying is a well-established process to fabricate ceramic coatings (Ref 3). Oxide ceramics are the most popular plasma spray coating materials which are usually employed for spraying in ambient atmosphere such as Al_2O_3, TiO_2, TiO_2-Al_2O_3, Cr_2O_3, and Y_2O_3-ZrO_2 (Ref 4). Availability of diverse ceramic materials benefits coating selections to fulfill different functional requirements from corrosion and wear protections to thermal barrier in different fields. For material protections from corrosion and wear, the coating is generally required to have a dense microstructure. However, it is well known that a thermally sprayed ceramic coating usually presents a lamellar structure with a certain amount of pores, including globular pores, interlamellar unbonded interface and vertical cracks in individual splats. Among globular pores and inter-lamellar pores, the later in the form of inter-splat unbonded interfaces play a significant role in the determination of coating properties (Ref 5). The existence of limited lamellar interface bonding as interlamellar pore in the ceramic coating was revealed by McPherson through TEM examination of microstructure of Al_2O_3 coating (Ref 6) and was then visualized through copper electroplating into alumina coating (Ref 7). This feature was also confirmed in the same way as copper plating into alumina coating in plasma-sprayed Ni-20Cr coating by infiltrating Bi alloy (Ref 8) and tungsten coating by infiltrating copper (Ref 9), respectively. In addition, intra-splat cracks are also usually observed within individual ceramic splats (Ref 10), which are generated by the intrinsic quenching stress (Ref 10, 11). The pores in the form of unbonded inter-splat interfaces and intra-splat cracks are usually interconnected through the whole coating, which allows easy penetration of a corrosive gaseous material or liquid matter to the coating/substrate interface as revealed by infiltrating experiments (Ref 7-9, 12-14). Therefore, the as-sprayed ceramic coating is not able to provide protection for a metal substrate against corrosion in corrosive environment. It is still a great challenge how to deposit a fully dense ceramic coating which can provide a metal substrate with excellent protection against corrosion besides excellent anti-wear resistance. On the other hand, the interface bonding dominates the coating physical and mechanical properties because a variety of coating properties are proportional to splat interface bonding ratio (Ref 5, 15, 16). Thus, a limited lamellar interface bonding sets up a low ceiling for properties of thermal spray coating in comparison with those of the identical bulk materials such as thermal or electrical conductivity, mechanical strength, or toughness, although a low thermal conductivity is expected for thermal barrier coating. For example, a linear relationship between fracture toughness along the lamellar direction and the lamellar bonding ratio (Ref 16) demonstrates a clearly such ceiling for fracture toughness based on the effect of spray parameters on interlamellar bonding ratio (Ref 5, 17). To improve the toughness of thermal spray ceramic coatings, many different approaches were attempted such as optimization of coating microstructures [18], multilayered coating design for durable TBCs [19, 20], and mimicking the nacre-like structure (Ref 21, 22). However, the most effective approach is to deposit a dense ceramic coating with fully bonded splats, since evidently the fracture toughness is proportional to lamellar bonding ratio both theoretically (Ref 16) and experimentally (Ref 16, 23). It has been a long-term challenge to design and deposit a ceramic coating with a controlled lamellar interface bonding ratio up to 100%.

It has been well understood qualitatively that increasing the substrate temperature during spraying leads to enhanced coating property due to improvement in the interlamellar bonding formation (Ref 11, 24, 25). Recent investigations revealed that there exists a critical deposition temperature, above which a ceramic molten droplet at a temperature above its melting point bonds completely to a solid substrate surface (Ref 17, 26). Here, the deposition temperature is referred to as the surface temperature of the coating prior to droplet impact during deposition. More important finding is that the critical bonding temperature is linearly proportional to the melting point of spray materials as shown in Fig. 1 (Ref 27). Based on such result, the critical bonding temperature theory can be proposed for control of splat bonding formation and deposition of a dense thermal spray ceramic coating with sufficiently bonded lamellae. This theory describes that the sufficient condition for spreading ceramic melt to bond fully to the previously deposited splat surface is that the melt/substrate interface temperature must be higher than the glass transition temperature of the spray material. To fulfill this condition, the coating surface temperature prior to molten ceramic droplet impact must be higher than the critical bonding temperature reported recently in the literature (Ref 27). Accordingly, it can be inferred that a dense ceramic coating with fully bonded splats can be deposited at room temperature in an ambient atmosphere when a ceramic material having a melting point lower than about 1500 °C is used. Although the bonding formation depends primarily on the mobility of atoms in a supercooled melt during splat cooling after a molten ceramic droplet impacts on the substrate (Ref 27), such concept can provide a useful guideline to develop coating materials which are deposited at room temperature for providing an effective protection against wear or corrosion.

Potassium titanate $K_2Ti_6O_{13}$ (KTO) of tunnel structure has more superior strength and reinforcement effect than glass fiber and carbon fiber, and thus, it has been used as reinforcement in metal, polymer, and ceramics (Ref 28-30).

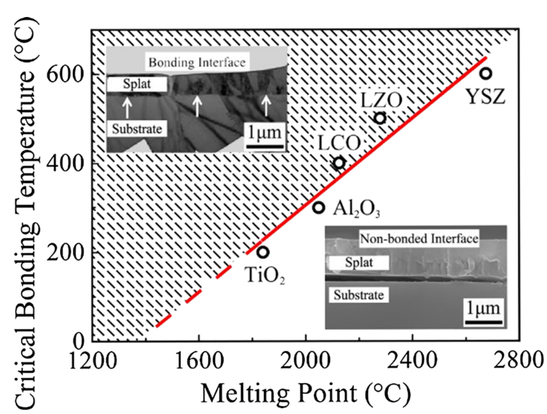

Fig. 1 Relationship between the critical deposition temperature for bonding formation and melting point of ceramic coating materials (Ref 27)

It also shows excellent performance as a functional material such as biocompatibility, photocatalytic performance for water splitting, and gas sensing, and as host structure for Li-ion batteries [31-34]. Moreover, it presents excellent corrosion resistance to alkali (Ref 35). Therefore, it could be a potential coating material for wide applications. More importantly, since potassium titanate $K_2Ti_6O_{13}$ has a melting point of ~ 1360 °C, it was selected in the present study for plasma spraying to validate the above concept. The bonding characteristics of $K_2Ti_6O_{13}$ molten droplets to ceramic substrate were investigated through splat deposition. The microstructure of plasma-sprayed $K_2Ti_6O_{13}$ coating and morphology of fractured coating were characterized to further reveal the lamellar interface bonding feature in the coating. Moreover, the $K_2Ti_6O_{13}$ coating was subjected to erosion to examine the effect of the lamellar interface bonding on coating performance since particle erosion of a plasma-sprayed ceramic coating is sensitive to interlamellar bonding.

Experimental

Materials and Coating Deposition Methods

The fine $K_2Ti_6O_{13}$ powders were agglomerated to fabricate thermal spray feedstocks. The agglomerated powders were then sintered at 1100 °C for 15 h. Figure 2 shows the morphology and cross-sectional microstructure of typical agglomerate-sintered KTO powders. It can be seen that the powder presents a near spherical morphology. After sintering at 1100 °C, the powder becomes dense although there were still some small pores inside the powder. X-ray diffraction (XRD) analysis revealed that powders have a rectangular tunnel structure with a nominal composition of $K_2Ti_6O_{13}$ (Fig. 3). In order to examine the effect of powder size on the coating formation, the powders were sieved into two particle size ranges: ~ 5-30 μm (fine powder) and 30-75 μm (coarse powder).

The coating was deposited on a sand-blasted stainless steel substrate. For examining the bonding formation of isolated splat, a surface-polished TiO_2 was used as the substrate. In order to obtain a clean surface without evaporative adsorbates and to ensure deposition of regular disk splat, the substrate at a preheated temperature of 110 °C by a copper heater was used to avoid moisture adsorption. Since some physical adsorbed water molecules could be completely desorbed at ~ 200 °C (Ref 36), the substrate was firstly preheated to 250 °C and then cooled down to 110 °C.

Plasma spraying was carried out at the conditions given in Table 1. Ar-H_2 plasma jet was used to accelerate and heat spray particles for generating a stream of molten droplets for coating deposition. A plasma torch traverse speed of 400 mm/s was used for coating deposition. In order to obtain completely distinguished isolating splats, a high torch traverse speed of 1200 mm/s was used for splat deposition.

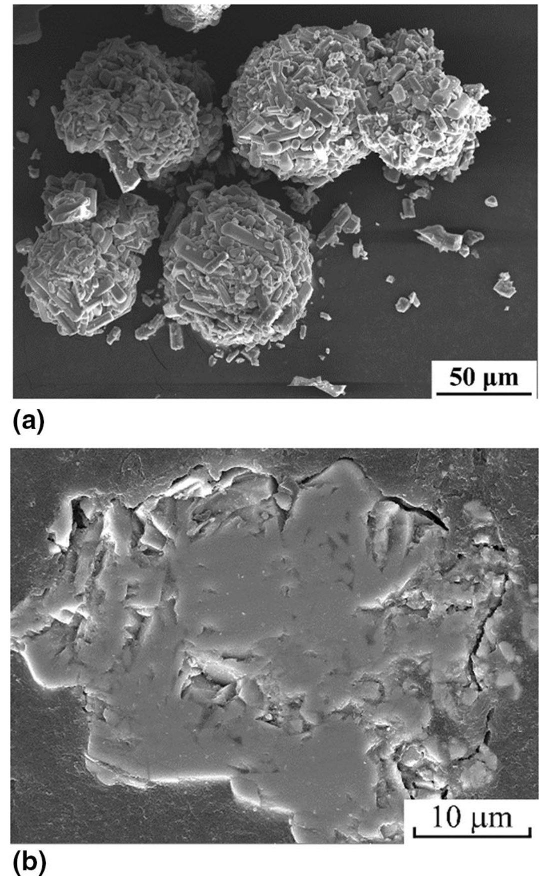

Fig. 2 Morphology and microstructure of KTO powder (30-75 μm). (a) As-agglomerated KTO powder. (b) Cross-sectional morphology and microstructure

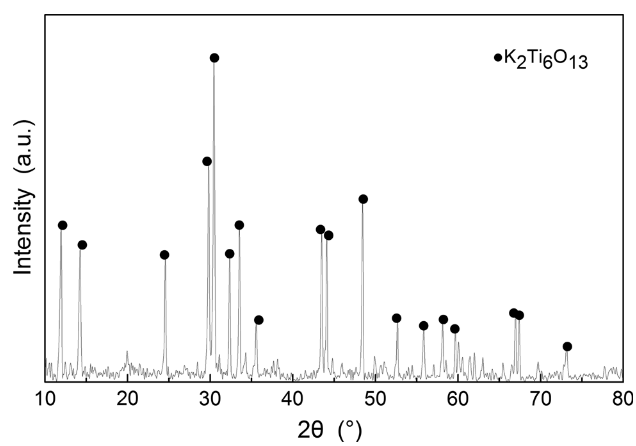

Fig. 3 X-ray diffraction pattern of KTO powder for plasma spraying

Table 1 Plasma spray conditions for KTO coating deposition

Spray parameter	Value
Spray distance, mm	80
Plasma arc power, kW	38
Arc current, A	750
Arc voltage, V	51
Plasma gas (Ar), L/min	45
Auxiliary gas (H_2), L/min	4
Torch traverse speed, mm/s	400, 1200

Characterization Methods

The splats were characterized by scanning electron microscopy (SEM) from surface and fractured cross sections. The fractured sample was used for examination of inter-splat bonding state.

The KTO coating was characterized through both the polished cross section and fractured cross sections by SEM. X-ray diffraction was used for phase characterization of the coating. Moreover, micro-hardness of KTO coating was tested at a load of 300 gf and 30-s loading time. Forty tests were made and the average hardness was calculated. The erosion test was conducted by successive feeding of 30 g abrasives at impact angles of 60° and 90°, respectively. Corundum particles with a nominal size of 250 μm were used as abrasives. The detailed erosion test conditions can be found elsewhere (Ref 37).

Results and Discussion

Typical Features of Plasma-Sprayed $K_2Ti_6O_{13}$ Splats

Through controlling the substrate preheating, regular disk splats were deposited. Figure 4(a) shows the morphology of KTO splat deposited on TiO_2 surface using fine KTO powder. A close examination revealed that such small-sized splat presents not only regular disk shape, but also excellent integrity without evident intra-splat cracks within the splat.

From the morphology of cross section of fractured KTO splat shown in Fig. 4(b), it is clear that no fracture or delamination occurred directly from the splat/substrate interface. Instead, the fracture from the inner of splat can be clearly observed from terrace fracture morphology on the cross section of fractured KTO splat. This fact reveals the formation of excellent bonding at the interface between KTO splat and TiO_2 substrate. On the other hand, the micro-cracks resulting from quenching stress were

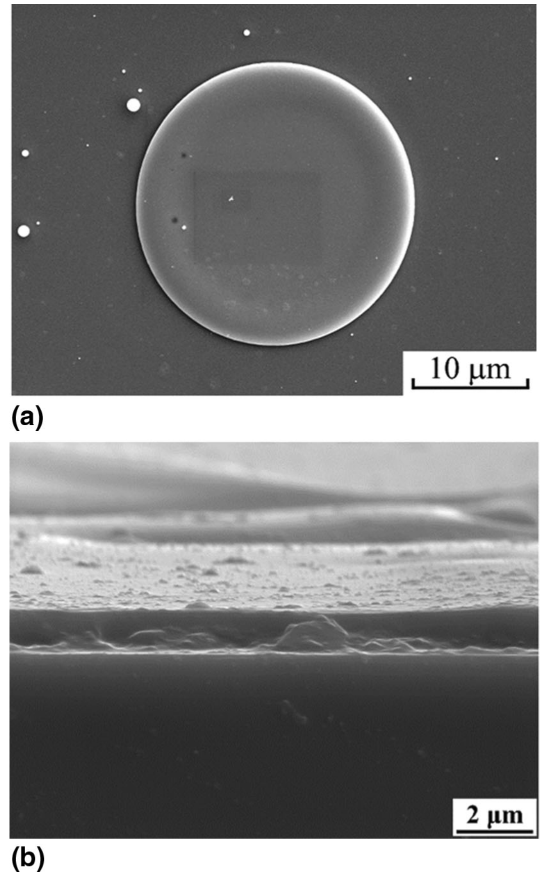

Fig. 4 Morphology of KTO splat deposited on flat TiO_2 and cross-sectional morphology of fractured KTO splat using fine KTO powder. (a) Surface morphology, (b) cross section

observed in the splat with a regular disk shape deposited by coarse powder. Moreover, voids were also observed within splat.

Microstructure of Plasma-Sprayed $K_2Ti_6O_{12}$ Coatings

Figure 5 shows the typical microstructure of plasma-sprayed KTO coating using fine KTO powder of a small size range from 5 to 30 μm. Although pores were present on the cross-sectional microstructure, the coating presents a dense microstructure as shown in Fig. 5(b).

A close examination reveals that, besides some pores in several micrometers marked by white arrows, some small pores marked by black arrows are present at the interface between splats. The formation of such pores is possibly related to the gases in molten KTO droplet which were retained from feedstock powder. This is because that during the solidification process the gas phase enclosed in droplet retained in splat as pores.

Figure 6 shows the typical microstructure of KTO coating deposited by using coarse powder with a size range

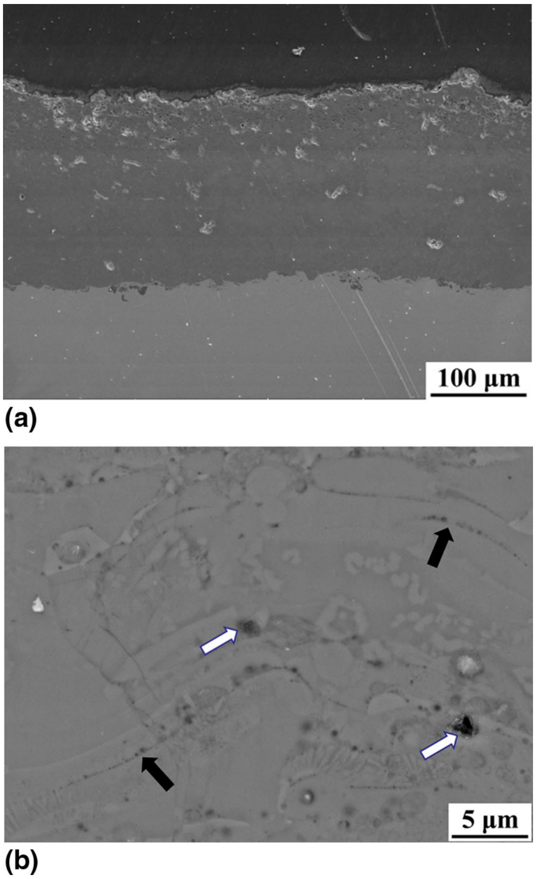

Fig. 5 Typical microstructure of KTO coating deposited using the powders with a size range from 5 to 30 µm at different magnifications. (a) Low magnification, (b) high magnification

from 30 to 75 µm. Globular pores in a large size were observed on the polished cross section of the coating. Those large pores in tens of micrometers might result from the fracture during sample preparation. Besides those large-sized pores, some small pores can be seen as shown in Fig. 6(b). Moreover, occasionally, cracks perpendicular to the deposition direction passing through several splats were observed, as shown in Fig. 6(c).

To reveal the bonding at the interfaces between splats in KTO coating, the coating was fractured in the direction perpendicular to the deposition direction (Fig. 7). For conventional plasma spray ceramic coating with limited lamellar interface bonding, fracturing could cause debonding from weakly bonded lamellar interfaces (Ref 17). Typical lamellar structure, which may not be observed from a polished cross section, can be clearly highlighted by fracturing the coating. However, from those images shown in Fig. 7, lamellar structure features, usually being observed for conventional plasma-sprayed ceramic coating, were not evidently present on the fractured cross sections. The fracture occurred in a way more like that occurs to

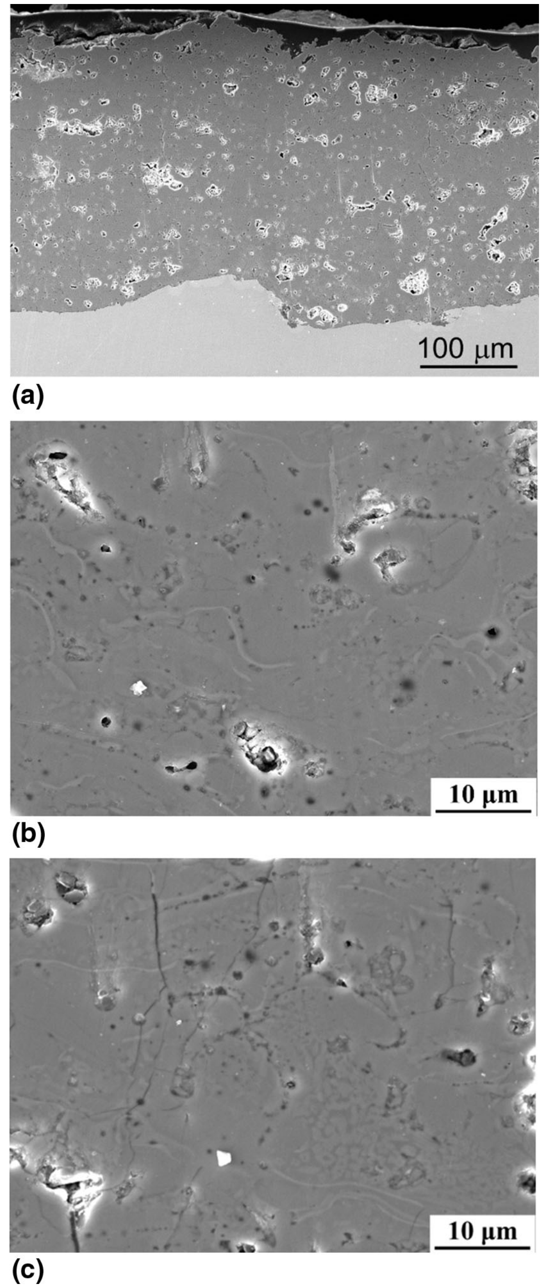

Fig. 6 Typical microstructure of KTO coating deposited by the powders with a size range from 30 to 75 µm at different magnifications. (a) Low magnification, (b) and (c) high magnification

sintered bulk ceramics. This means that deposited lamellae have been fully bonded together in the coating.

Moreover, it is interesting to notice that the microcracks in individual splats were not observed at the fractured cross section as shown in Fig. 7(b) and (c). A close examination reveals the existence of pores in the coating. Some pores, marked by white arrows, are in a size up to several micrometers (Fig. 7b). Many pores, marked by white arrows, are in a size of submicrometers. It can be also noticed that most pores have a spherical shape, being

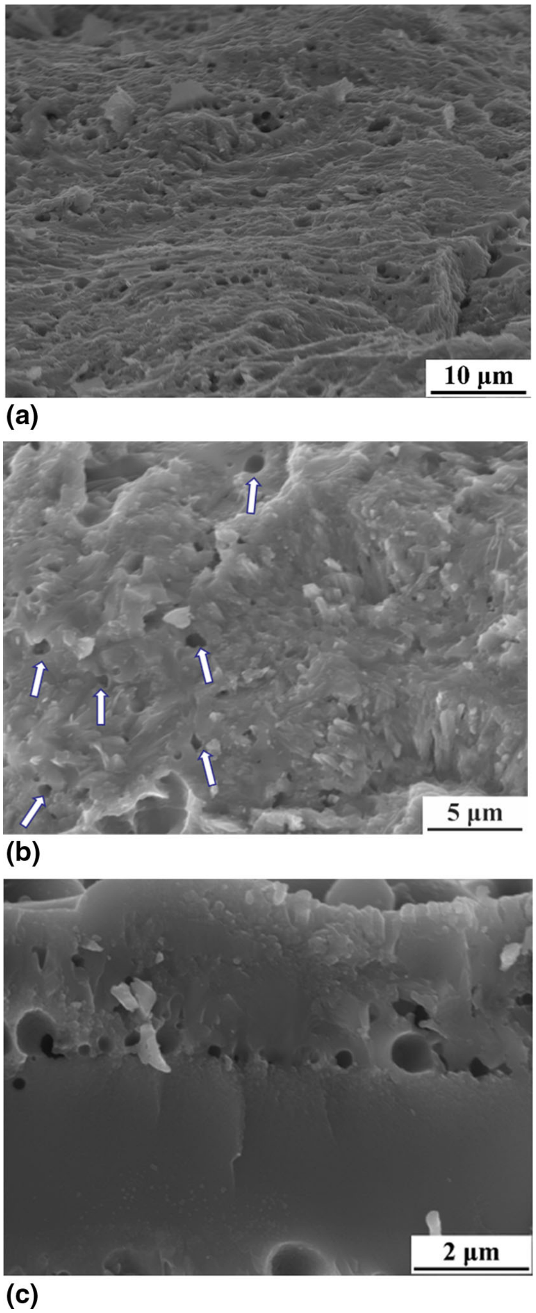

Fig. 7 Cross-sectional morphology of fractured KTO coating deposited by coarse powder. (a) Low magnification, (b) and (c) high magnification

consistent with those in Fig. 5. Figure 7(c) clearly shows that some pores of spherical shape are present near the interface between splats. This fact indicates that pores have formed in molten splat from gas phase, being possibly evolved during solidification of spreading melt and/or gas enclosed in molten droplet due to pores in powder, although the evolution of gas phases needs further investigation.

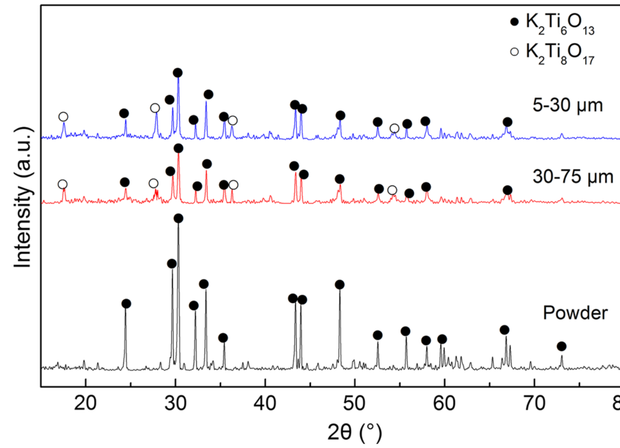

Fig. 8 XRD patterns of two KTO coatings deposited by two powders in different particle size ranges

Figure 8 shows XRD patterns of KTO coatings deposited by powders of two different size ranges in comparison with that of powder. The coating consists mainly of $K_2Ti_6O_{13}$ phase. It was reported that the cooling rate of melt influences little $K_2Ti_6O_{13}$ phase formation rather than melt composition (Ref 38) although the cooling rate during plasma spraying may be much larger than that reported in the above literature during pouring $K_2Ti_6O_{13}$ melt on a water-cooled steel plate. The main $K_2Ti_6O_{13}$ phase was retained from powder. This fact suggests that during rapid heating in high-temperature plasma and subsequent splat quenching $K_2Ti_6O_{13}$ phase is stable. However, a small amount of $K_2Ti_8O_{17}$ phase was present in the coatings. The intensity of the main peak of $K_2Ti_8O_{17}$ phase in the coating deposited by small powders is relatively higher than that in the coating by large powder. During plasma spraying, particles are heated to temperatures higher than their melting point. The vaporization of a component with high vapor pressure or low melting point or low boiling point in multi-component ceramic may preferentially occur (Ref 39). Such vaporization causes the deviation of compound compositions from its stoichiometry. Significant loss of element will lead to new phase formation (Ref 40). When $K_2Ti_6O_{13}$ powders are heated to molten state by plasma jet, vaporization of potassium may occur, which leads to the formation of potassium titanate $K_2Ti_8O_{17}$ with low potassium content. Since the smaller the particle size the higher temperature the particle is heated. A higher temperature results in more preferential vaporization of molten droplet. When smaller $K_2Ti_6O_{13}$ powders are used, higher temperature of molten droplets may lead to higher loss of potassium and consequently the formation of higher amount of $K_2Ti_8O_{17}$ phase with a low content of potassium. Therefore, for KTO coatings, the formation of $K_2Ti_8O_{17}$ can be attributed to the vaporization of potassium during plasma spraying.

Typical Properties of Plasma-Sprayed $K_2Ti_6O_{13}$ Coatings

The hardness can be used as a general indication of the coating mechanical property. Due to the anisotropic feature of lamellar microstructure, the properties of thermally sprayed ceramic coating are often anisotropic. For example, Young's modulus in the in-plane direction is often much larger than that in the off-plane direction (Ref 41-43). The hardness test of KTO coating yielded the mean microhardnesses of 454 ± 107 and 454 ± 156 Hv from the polished cross section and the polished surface, respectively. The average hardness of the coating in both the directions is almost the same. This fact means that plasma-sprayed KTO coating presents a homogeneous microstructure, which is different from the typical lamellar microstructure of other plasma-sprayed ceramic coatings. This feature is attributed to a dense microstructure, especially with well-bonded lamellae.

Since particle erosion of thermally sprayed ceramic coating is sensitive to lamellar interface bonding, the erosion test was performed for KTO coating at impact angles of 60° and 90°. Figure 9 shows that the erosion weight loss of the coating is proportional to the weight of abrasives, as observed for other ceramic coatings (Ref 37). The erosion test of KTO coating at 90° yielded an erosion rate of 2.1 mg/g, which is much lower than that of Al_2O_3 coatings plasma-sprayed at room temperature (Ref 37, 44). However, the KTO coating hardness (about 450 Hv) is much lower than that of Al_2O_3 coatings (typically 800-1400 Hv) (Ref 45-47).

In order to examine the erosion mechanism of the KTO coating with a dense structure, the surface morphologies of the KTO coating before and after erosion test are compared, as shown in Fig. 10(a) and (b). Figure 10(a) presents a typical splat stacking structure for the as-sprayed KTO coating. Except some splashed small particles, the splats exhibited a quite smooth surface profile. However, the coating surface after erosion test presents a fairly rough surface morphology with some indentations caused by high-velocity alumina abrasive particles. This surface morphology is far different from conventional eroded surface of plasma-sprayed alumina coatings which have been reported in the literature (Ref 37, 44). For typical plasma-sprayed ceramic coatings with a lamellar structure, the interlamellar pores act as pre-cracks during erosion test. As a result, the splats peel off resulting from the propagation of those pre-cracks under repeated impacts of abrasives particles, and thereby, the underlying splats are exposed to serve as newly bared surface with a similar smooth surface profile to splat (Ref 37, 44). However, the KTO coating with a dense microstructure presents a much different erosion mechanism from conventional plasma-sprayed ceramic coatings with a lamellar structure.

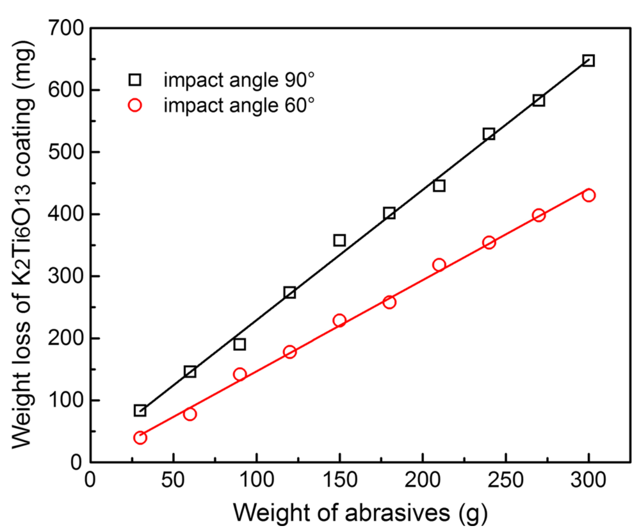

Fig. 9 Change in erosion weight loss of $K_2Ti_6O_{13}$ coating with an increase in the weight of abrasives

To further probe the material loss mechanism of dense KTO coating, the cross-sectional morphology of KTO coating after the erosion test was examined as shown in Fig. 10(c) and (d). The cross-sectional morphology of dense KTO coating revealed no evident subsurface cracking, preferentially along lamellar interfaces in the in-plane direction, while such in-plane cracking is usually observed for thermally sprayed coatings with limited lamellar interface bonding (Ref 44). This fact provides further evidence that the lamellae in the present coating are well bonded to each other, avoiding the guiding effect of unbonded interfaces as pre-cracks in conventional thermally sprayed ceramic coating (Ref 37). By this way, the KTO coating with a dense microstructure presents excellent erosion resistance like bulk material and therefore even presents a much higher erosion resistance than plasma-sprayed Al_2O_3 coatings with a lamellar structure but a much higher hardness. Therefore, based on the relationship between the critical bonding temperature and materials melting point (Ref 27), selecting low melting point ceramic materials is a powerful coating design approach to prepare ceramic coatings with better performance such as excellent erosion resistance.

Effect of Materials Type on the Bonding Formation During Molten Droplet Impact

It had been known for long that thermal spray ceramic coatings deposited at conventional routine present a lamellar structure with limited interface bonding (Ref 6, 17). The ceramic coatings usually present a mean bonding ratio less than one-third of total apparent interface

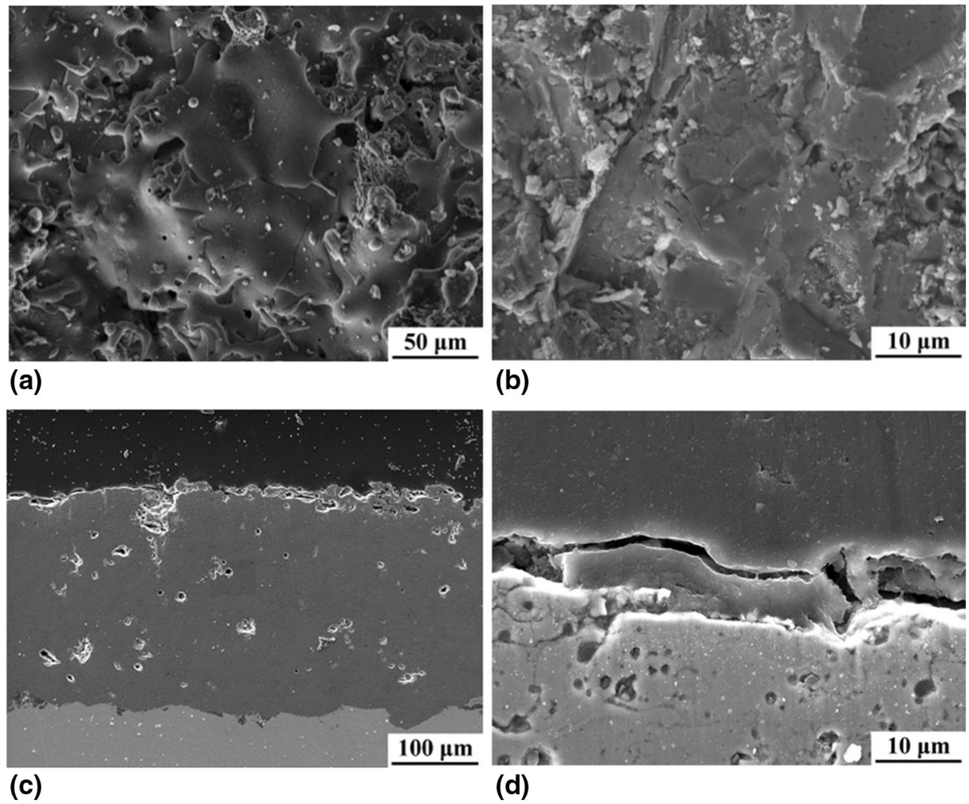

Fig. 10 Surface morphologies and cross-sectional morphologies of $K_2Ti_6O_{13}$ coating before/after erosion test at 90°. (a) Surface morphology of as-sprayed coating presenting a lamellar stacking structure, (b) surface morphology of the coating after erosion test, (c) and (d) cross-sectional morphologies of coating after erosion test

area, which was observed directly (Ref 5, 7, 17, 48) or estimated based on structure–property relationship models (Ref 6, 15). It was clearly recognized that molten droplet temperature contributes significantly the bonding formation upon molten droplet impact through systematical investigations (Ref 17), which was evidently proved by positive effect of deposition temperature on inter-splat bonding formation (Ref 11, 24, 25). Accordingly, with the increase in molten spray particle temperature the interface temperature between spreading melt and the substrate increases and subsequently the improved wetting enhances the bonding formation between spreading melt and substrate. However, it is well recognized that the molten ceramic spray particles can only be heated by plasma jet during plasma spraying to a temperature around its melting point with a limited overheating (Ref 49). Therefore, it is generally difficult to increase lamellar bonding ratio for common ceramic spray materials such as YSZ and Al_2O_3 by optimization of spray conditions.

Thermal spray deposition involves rapid quenching process (Ref 11). Splat is formed by rapid crystallization from significantly undercooled melt. The mobility of atoms or molecules in an undercooled melt decreases with the increase in the undercooling degree. The recent investigations evidently suggest that the inter-splat bonding can form when the molecules in the supercooling molten droplet in contact with ceramic substrate have certain mobility prior to its solidification (Ref 27). The mobility of molecules in melt to form chemical bond with the atoms on substrate surface will be lost when the melt is being supercooled to a temperature lower than its glass transition temperature since the viscosity of the supercooled melt decreases rapidly by several orders of magnitude (Ref 50). A higher interface temperature between spreading droplet and solid ceramic substrate than glass transition temperature benefits the bonding formation. As it was found recently, when the deposition temperature exceeds the critical deposition temperature for the bonding formation for a certain ceramic material, a higher interface temperature between melt and substrate can be reached than its glass transition temperature (Ref 27). As a result, the spreading ceramic molten droplet with a temperature higher than its melting point can form the bonding with the ceramic substrate surface at a temperature higher than the critical bonding temperature. It was also found that the critical bonding temperature is proportional to the melting point of spray material as shown in Fig. 1 (Ref 27). This fact means that materials type influences significantly the inter-splat bonding formation. Based on the relationship shown in Fig. 1, the correlation between the critical bonding temperature and the material melting point can be expressed by the following equation:

$$T_{\mathrm{d}} = 0.58 \times T_{\mathrm{m}} - 890$$

where T_d (°C) is the critical deposition temperature for splat bonding formation, i.e., the critical bonding temperature, and T_m is the melting point of spray material (°C).

Thus, from the melting point of KTO, its critical bonding temperature is estimated to be ~ -100 °C. The corresponding interface temperature when a KTO droplet at its melting point impacts is about the glass transition temperature of KTO, being $\sim$ 816 °C estimated in the same way in the literature (Ref 27). Therefore, since with a ceramic substrate surface at ambient temperature, the deposition temperature is $\sim$ 120 °C higher than its critical bonding temperature, the maximum KTO melt/substrate interface temperature becomes about 120 °C higher than its glass transition temperature. Thus, the mobility of molecules in KTO melt is sufficiently high to coordinate their positions for the bonding formation at the interface. As a result, impacting KTO molten ceramic droplet can certainly bond to the underlying KTO ceramic surface as revealed in the present study. Moreover, the present results clearly show that following the results reported in the literature (Ref 27) for ceramic spray materials with lower melting point than 1500 °C, plasma spraying at room temperature even following the conventional spraying routine can yield a dense coating with well-bonded lamellae.

Conclusions

$K_2TiO_6O_{13}$ was used as a typical ceramic coating material to prove the concept that a dense ceramic coating with well-bonded lamellae can be thermally sprayed at room temperature in ambient atmosphere by using the ceramic materials having a melting point lower than about 1500 °C. The KTO coatings presented a dense microstructure without typical lamellar features. Some pores are present in the coating which are possibly formed from absorbed gases at high-temperature molten state. Results showed that splats deposited at 110 °C in ambient atmosphere were fully bonded to TiO_2 substrate. The fracture surface of the coating evidently indicates that all splats were fully bonded together. This fact was further confirmed by the erosion test. Hardness test from both the cross section and the surface yielded the same value for KTO coating, indicating isotropic characteristic resulting from excellent lamellar interface bonding. As a result, a dense ceramic coating with fully bonded lamellae can be deposited at a deposition temperature of room temperature in ambient atmosphere.

Acknowledgments The present project is financially supported by National Science Foundation (No. 51171144) and the National Basic Research Program of China (No. 2012CB625104).

References

1. A. Vardelle, C. Moreau, J. Akedo et al., The 2016 Thermal Spray Roadmap, *J. Therm. Spray Technol.*, 2016, **25**(8), p 1376-1440
2. A. McWilliams, *High-Performance Ceramic Coatings: Markets and Technologies*, BBC Research, 2016
3. J.R. Davis, *Handbook of Thermal Spray Technology*, ASM International, Materials Park, 2004
4. L. Pawlowski, *The Science and Engineering of Thermal Spray Coatings*, Wiley, Chichester, 1995
5. C.-J. Li and A. Ohmori, Relationship Between the Structure and Properties of Thermally Sprayed Deposits, *J. Therm. Spray Technol.*, 2002, **11**, p 365-374
6. R. McPherson and B.V. Shafer, Interlamellar Contact Within Plasma-Sprayed Coatings, *Thin Solid Films*, 1982, **97**, p 201-204
7. A. Ohmori and C.-J. Li, Quantitative Characterization of the Structure of Plasma Sprayed Al_2O_3 Coating by Using Copper Electroplating, *Thin Solid Films*, 1991, **201**, p 241-252
8. S. Kuroda, T. Dendo, and S. Kitahara, Quenching Stress in Plasma Sprayed Coatings and Its Correlation with the Deposit Microstructure, *J. Therm. Spray Technol.*, 1995, **4**(1), p 75-84
9. S. Boire-Lavigne, C. Moreau, and R.G. Saint-Jacques, The Relationship Between the Microstructure and Thermal Diffusivity of Plasma-Sprayed Tungsten Coatings, *J. Therm. Spray Technol.*, 1995, **4**(3), p 261-267
10. L. Chen, G.J. Yang, C.-X. Li, and C.-J. Li, Edge Effect on Crack Patterns in Thermally Sprayed Ceramic Splats, *J. Therm. Spray Technol.*, 2017, **26**(3), p 302-314
11. S. Kuroda and T.W. Clyne, The Quenching Stress in Thermally Sprayed Coating, *Thin Solid Films*, 1991, **200**, p 49-66
12. Y. Arata, A. Ohmori, and C.-J. Li, Electrochemical Method to Evaluate the Connected Porosity in Ceramic Coatings, *Thin Solid Films*, 1988, **156**, p 315-325
13. M. Vippola, J. Vuorinen, P. Vuoristo, T. Lepisto, and T. Mantyla, Thermal Analysis of Plasma Sprayed Oxide Coatings Sealed with Aluminium Phosphate, *J. Eur. Ceram. Soc.*, 2002, **22**, p 1937-1946
14. C.-J. Li, X.-J. Ning, and C.-X. Li, Effect of Densification Process on the Properties of Plasma-Sprayed YSZ Electrolyte Coatings for Solid Oxide Fuel Cell, *Surf. Coat. Technol.*, 2005, **190**, p 60-64
15. R. McPherson, A Model for the Thermal Conductivity of Plasma-Sprayed Ceramic Coatings, *Thin Solid Films*, 1984, **112**, p 89-95
16. C.-J. Li, W.-Z. Wang, and Y. He, Dependency of Fracture Toughness of Plasma-Spray Al_2O_3 Coatings on Lamellar Structure, *J. Therm. Spray Technol.*, 2004, **13**(3), p 425-443
17. C.-J. Li, G.J. Yang, and C.X. Li, Development of Particle Interface Bonding in Thermal Spray Coatings: A Review, *J. Therm. Spray Technol.*, 2013, **22**(2-3), p 192-206
18. G. Dwivedi, V. Viswanathan, S. Sampath, A. Shyam, and E. Lara-Curzio, Fracture Toughness of Plasma-Sprayed Thermal Barrier Ceramics: Influence of Processing, Microstructure, and Thermal Aging, *J. Am. Ceram. Soc.*, 2014, **97**(9), p 2736-2744
19. C.-J. Li, Y. Li, G.-J. Yang, and C.-X. Li, A Novel Plasma-Sprayed Durable Thermal Barrier Coating with the Well-Bonded YSZ Interlayer Between Porous YSZ and Bond Coat, *J. Therm. Spray Technol.*, 2012, **21**, p 383-390
20. V. Viswanathan, G. Dwivedi, and S. Sampath, Engineered Multilayer Thermal Barrier Coatings for Enhanced Durability and Functional Performance, *J. Am. Ceram. Soc.*, 2014, **97**(9), p 2770-2778
21. G. Dwivedi, K. Flynn, M. Resnick, S. Sampath, and A. Gouldstone, Bioinspired Hybrid Materials from Spray-Formed Ceramic Templates, *Adv. Mater.*, 2015, **27**(19), p 3073-3078

22. J. Rong, K. Yang, Y. Zhuang, J. Ni, H. Zhao, S. Tao, X. Zhong, and C. Ding, Phase and Microstructure Evolution and Toughening Mechanism of a Hierarchical Architectured Al_2O_3-Y_2O_3 Coating Under High Temperature, *J. Therm. Spray Technnol.*, 2018, **27**, p 358-370
23. Y.-Z. Xing, C.-J. Li, C.-X. Li, and G.-J. Yang, Relationship Between the Interlamellar Bonding and Properties of Plasma-Sprayed Y_2O_3-ZrO_2 Coatings, *Thermal Spray 2009: Expanding Thermal Spray Performance to New Markets and Applications*, B.R. Marple, M.M. Hyland, Y.-C. Lau, C.-J. Li, R.S. Lima, and G. Montavon, Ed., ASM International, Materials Park, 2009, p 939-944
24. H.B. Guo, R. Vaßen, and D. Stöver, Atmospheric Plasma Sprayed Thick Thermal Barrier Coatings with High Segmentation Crack Density, *Surf. Coat. Technol.*, 2004, **186**, p 353-363
25. Y.Z. Xing, C.J. Li, Q. Zhang, C.X. Li, and G.J. Yang, Influence of Microstructure on the Ionic Conductivity of Plasma-Sprayed Yttria-Stabilized Zirconia Deposits, *J. Am. Ceram. Soc.*, 2008, **91**(12), p 3931-3936
26. G.J. Yang, C.X. Li, S. Hao, Y.Z. Xing, Y.Z. Xing, and C.-J. Li, Critical Bonding Temperature for the Splat Bonding Formation During Plasma Spraying of Ceramic Materials, *Surf. Coat. Technol.*, 2013, **235**, p 841-847
27. S.W. Yao, C.-J. Li, J.J. Tian, G.J. Yang, and C.X. Li, Conditions and Mechanisms for the Bonding of a Molten Ceramic Droplet to a Substrate After High-Speed Impact, *Acta Mater.*, 2016, **119**, p 9-25
28. R. Murakami and K. Matsui, Evaluation of Mechanical and Wear Properties of Potassium Acid Titanate Whisker-Reinforced Copper Matrix Composites Formed by Hot Isostatic Pressing, *Wear*, 1996, **201**, p 193-198
29. D. Yu, J. Wu, L. Zhou, D. Xie, and S. Wu, The Dielectric and Mechanical Properties of a Potassium-Titanate-Whisker-Reinforced PP/PA Blend, *Compos. Sci. Technol.*, 2000, **60**, p 499-508
30. Z. Lu, Y. Liu, B. Liu, and M. Liu, Friction and Wear Behavior of Hydroxyapatite Based Composite Ceramics Reinforced with Fibers, *Mater. Des.*, 2012, **39**, p 444-449
31. Y. Qi, Y. He, C. Cui, S. Liu, and H. Wang, Fabrication and Biocompatibility In Vitro of Potassium Titatnate Biological Thin/Titanium Alloy Biological Composite, *Front. Mater. Sci.*, 2007, **1**, p 252-257
32. H. Yoshida, M. Takeuchi, M. Sato, L. Zhang, T. Teshima, and M.G. Chaskar, Possium Hexatitanate Photocatalysts Prepared by Flux Method for Water Splitting, *Catal. Today*, 2014, **232**, p 158-164
33. A.S. Varezhnikov, F.S. Fedorov, I.N. Burmistrov, I.A. Plugin, M. Sommer, A.V. Lashkov, A.V. Gorokhovsky, A.G. Nasibulin, D.V. Kuznetsov, M.V. Gorshenkov, and V.V. Sysoev, The Room-Temperature Chemiresistive Properties of Potassium Titanate Whiskers Versus Organic Vapor, *Nanomaterials*, 2017, **7**, p 455-465
34. R. Dominiko, L. Dupond, M. Gabersaek, J. Jamnik, and E. Baudrin, Alkali Hexatitanate-$A_2Ti_6O_{13}$ (A = Na, K) as Host Structure for Reversible Lithium Insertion, *J. Power Sources*, 2007, **174**, p 1172-1176
35. X. Cheng, Q. Dong, Z. Li, X. Guo, and W. Duan, Influence of Potassium Titanate Whisker on the Mechanical Properties and Microstructure of Calcium Aluminate Cement for In Situ Combustion, *J. Adhes. Sci. Technol.*, 2018, **32**, p 343-358
36. C.J. Li and J.L. Li, Evaporated-Gas-Induced Splashing Model for Splat Formation during Plasma Spraying, *Surf. Coat. Technol.*, 2004, **184**(1), p 13-23
37. S.W. Yao, G.J. Yang, C.X. Li, and C.J. Li, Improving Erosion Resistance of Plasma-Sprayed Ceramic Coatings by Elevating the Deposition Temperature Based on the Critical Bonding Temperature, *J. Therm. Spray Technol.*, 2018, **27**(1-2), p 25-34
38. P. Ponce-Pena, M.A. Gozalez-Lozano, M.A. Escobedo-Bretado, P. de Lira-Gomez, E. Garcia-Sanchez, E. Rivera, and L. Alexandrova, Synthesis and characterization of Potassium Hexatitanate Using Boric Acid as the Flux, *Ceram. Int.*, 2015, **41**, p 10051-10056
39. L.S. Wang, S.L. Zhang, T. Liu, C.J. Li, C.X. Li, and G.J. Yang, Dominant Effect of Particle Size on the CeO_2 Preferential Evaporation During Plasma Spraying of $La_2Ce_2O_7$, *J. Eur. Ceram. Soc.*, 2017, **37**(4), p 1577-1585
40. S. Zhang, T. Liu, C. Li, S. Yao, and C. Li, Atmospheric Plasma-Sprayed $La_{0.8}Sr_{0.2}Ga_{0.8}Mg_{0.2}O_3$ Electrolyte Membranes for Intermediate-Temperature Solid Oxide Fuel Cells, *J. Mater. Chem. A*, 2015, **3**(14), p 7535-7553
41. S.H. Leigh, C.K. Lin, and C.C. Berndt, Elastic Response of Thermal Spray Deposits Under Indentation Tests, *J. Am. Ceram. Soc.*, 1997, **80**, p 2093-2099
42. F. Kroupa, Nonlinear Behavior in Compression and Tension of Thermally Sprayed Ceramic Coatings, *J. Therm. Spray Technol.*, 2007, **16**(1), p 84-95
43. G.-R. Li, H. Xie, G.-J. Yang, G. Liu, C.-X. Li, and C.-J. Li, A Comprehensive Sintering Mechanism for TBCs-Part I: An Overall Evolution with Two-Stage Kinetics, *J. Am. Ceram. Soc.*, 2017, **100**(5), p 2176-2189
44. C.-J. Li, G.-J. Yang, and A. Ohmori, Relationship Between Particle Erosion and Lamellar Microstructure for Plasma Sprayed Alumina Coatings, *Wear*, 2006, **260**(11-12), p 1166-1172
45. A. Kobayashi, Enhancement of Functional Ceramic Coating Performance by Gas Tunnel Type Plasma Spraying, *J. Therm. Spray Technol.*, 2016, **25**(3), p 411-418
46. R.J. Damani and P. Makroczy, Heat Treatment Induced Phase and Microstructural Development in Bulk Plasma Sprayed Alumina, *J. Eur. Ceram. Soc.*, 2000, **20**(7), p 867-888
47. T. Chraska, Z. Pala, R. Musalek, J. Medricky, and M. Vilemova, Post-Treatment of Plasma-Sprayed Amorphous Ceramic Coatings by Spark Plasma Sintering, *J. Therm. Spray Technol.*, 2015, **24**(4), p 637-643
48. A. Ohmori, C.-J. Li, and Y. Arata, Influence of Plasma Spray Conditions on the Structure of Al_2O_3 Coatings, *Trans. Jpn. Weld. Res. Inst.*, 1990, **19**, p 259-270
49. M. Vardelle, A. Vardelle, and P. Fauchais, Study of Trajectories and Temperatures of Powders in a D.C. Plasma Jet—Correlation with Alumina Sprayed Coatings. *Proceedings of the 10th International Thermal Spraying Conference*, Essen, May 1983, German Welding Society, 1983, p 88-92
50. L.-M. Martinez and C. Angell, A Thermodynamic Connection to the Fragility of Glass-Forming Liquids, *Nature*, 2001, **410**, p 663-667